BIOCHEMISTRY
including biophysical chemistry & molecular biology

Article

pubs.acs.org/biochemistry

Contribution of Partial Charge Interactions and Base Stacking to the Efficiency of Primer Extension at and beyond Abasic Sites in DNA

Shuangluo Xia,[†] Ashwani Vashishtha,[†] David Bulkley,[†] Soo Hyun Eom,[‡] Jimin Wang,*[,†] and William H. Konigsberg*[,†]

[†]Department of Molecular Biophysics and Biochemistry, Yale University, New Haven, Connecticut 06520-8114, United States
[‡]School of Life Sciences, Gwangju Institute of Science and Technology, Buk-gu, Gwangju 500-712, Republic of Korea

Supporting Information

ABSTRACT: During DNA synthesis, base stacking and Watson–Crick (WC) hydrogen bonding increase the stability of nascent base pairs when they are in a ternary complex. To evaluate the contribution of base stacking to the incorporation efficiency of dNTPs when a DNA polymerase encounters an abasic site, we varied the penultimate base pairs (PBs) adjacent to the abasic site using all 16 possible combinations. We then determined pre-steady-state kinetic parameters with an RB69 DNA polymerase variant and solved nine structures of the corresponding ternary complexes. The efficiency of incorporation for incoming dNTPs opposite an abasic site varied between 2- and 210-fold depending on the identity of the PB. We propose that the A rule can be extended to encompass the fact that DNA polymerase can bypass dA/abasic sites more efficiently than other dN/abasic sites. Crystal structures of the ternary complexes show that the surface of the incoming base was stacked against the PB's interface and that the kinetic parameters for dNMP incorporation were consistent with specific features of base stacking, such as surface area and partial charge–charge interactions between the incoming base and the PB. Without a templating nucleotide residue, an incoming dNTP has no base with which it can hydrogen bond and cannot be desolvated, so that these surrounding water molecules become ordered and remain on the PB's surface in the ternary complex. When these water molecules are on top of a hydrophobic patch on the PB, they destabilize the ternary complex, and the incorporation efficiency of incoming dNTPs is reduced.

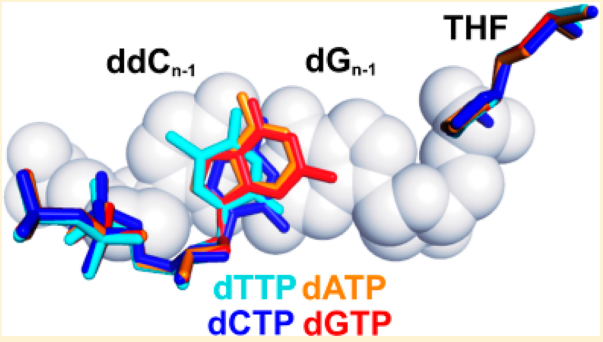

A basic sites are the most common lesions found in DNA. They occur under physiological conditions, with up to 10000 abasic sites formed in each cell per day because of spontaneous hydrolysis of the N-glycosidic bond between the base and the deoxyribosyl moiety.[1−4] In most cases, these lesions are rapidly removed via base excision repair (BER) pathways.[5] Left unrepaired, abasic sites provide strong blocks to DNA synthesis due to the lack of a templating base to instruct correct nucleotide incorporation.[6−9] In the absence of coding information, most replicative polymerases preferentially incorporate dAMP opposite an abasic site. This strong preference for dATP is known as the "A rule".[8,10−20] However, the mechanistic basis for the A rule still remains elusive despite the large number of kinetic and structural studies that have been reported on noninstructive lesion bypass or translesion synthesis by DNA polymerases.[21−23] It has been suggested that the preference for A is due to the fact that purines stack better than pyrimidines;[24,25] however, this explanation does not account for why A is inserted more efficiently than G. If the extent of base stacking alone was the only determining factor for insertion of dNTP opposite an abasic site, then dGTP should be incorporated as efficiently as dATP. Because this does not happen with most DNA pols, it implies that there are other interactions between the incoming dNTP and the PB (for the location of the PB in the primer–template sequence, see Figure 1A) that influence the efficiency of incorporation of a dNMP opposite an abasic site.

Reineks and Berdis[26] have identified a non-natural dNTP analogue, 5-nitro-1-indolyl-2′-deoxyriboside 5′-triphosphate (5-NITP), that was incorporated opposite an abasic site 1000-fold more efficiently than dAMP by T4 DNA polymerase (T4pol), a close relative of RB69pol. Because the size and shape of 5-NITP and dATP are similar, the large increase in incorporation efficiency was attributed to the nitro group at position 5 on the indole ring of 5-NITP. Presumably, it provides stronger $\pi-\pi$ interactions between the incoming nucleotide analogue and the aromatic amino acid side chains present in the NPB compared to the case in which the incoming dNTP was dATP. This explanation was deemed insufficient and required modification when the ternary complex, which had 5-NITP opposite an abasic site, was determined.[27] In addition to enhanced $\pi-\pi$ stacking interaction, there appeared to be a positive

Received: March 1, 2012
Revised: May 2, 2012
Published: May 25, 2012

dx.doi.org/10.1021/bi300296q | *Biochemistry* 2012, 51, 4922–4931

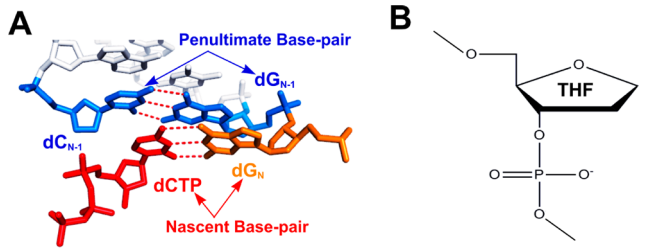

Figure 1. Nascent/penultimate base pairs and an abasic analogue. (A) Illustration of the positions of the nascent base pair (NB) and the penultimate base pair (PB) in the NBP. (B) Structure of tetrahydrofuran (THF) in DNA.

contribution from dipole−dipole interactions between the nitro group of 5-NITP and N4 of the cytosine residue situated 3′ to the abasic site in the template strand.[27] This result demonstrated that base stacking and $\pi-\pi$ interactions were only part of the reason that 5-NITP was inserted more efficiently than dATP when it was opposite an abasic site. It should be noted that the extent of this preference appears to be dependent on the particular DNA polymerase. For example, when 5-NITP was opposite an abasic site in the presence of Klenow fragment, there was only a small difference in the insertion efficiency of 5-NITP compared to that of dATP.[26] Whereas in our attempts to understand more about how this selectivity is achieved with a B family DNA polymerase, we used RB69pol and primer−template with tetrahydrofuran (THF, Figure 1B) as a stable abasic site mimic, an analogue has almost always been used in studies of translesion synthesis by DNA polymerases.[16,22,28−31]

After placing a THF in the templating position, we determined pre-steady-state kinetic parameters for all four incoming dNTPs with wild-type (wt) RB69pol, in an exo$^-$ background, and with an exo$^-$ RB69pol triple mutant (tm) that included the Y567A, L561A, and S565G substitutions. We designed this mutant so that it had the same pre-steady-state kinetic parameters as wt RB69pol for insertion of correct dNTPs, although it had reduced base selectivity.[32] Most importantly, this RB69pol mutant allowed us to capture relevant ternary complexes with THF in the templating position for crystallographic studies and made it possible to correlate and rationalize the kinetic behavior with structures of the corresponding ternary complexes. In addition, for each incoming dNTP, we varied the identity of the PB employing all 16 base pair combinations. Although the kinetics for incorporation of dNMPs opposite an abasic site by T4 pol have been studied previously without varying the PB's identity,[26,29,31,33−35] the results could not be fully explained solely by differences in base stacking or desolvation when insertion efficiencies of the incoming dNTPs were compared.[31,33−35] Our kinetic data and structural results show that, while base stacking is important, partial charge interactions between the incoming dNTP and the interface of the PB contribute significantly to the pre-steady-state kinetic parameters for the insertion of dNMP opposite an abasic site in the context of the tm RB69pol. We also propose that the A rule can be extended to include the observation that B family DNA polymerases, as exemplified by RB69pol and Phi29pol, can bypass dA/abasic sites more efficiently than any other dN/abasic lesion.

EXPERIMENTAL PROCEDURES

Chemicals. All chemicals were of the highest quality commercially available; dNTPs were purchased from Roche (Roche Applied Science, Indianapolis, IN). [γ-^{32}P]ATP was purchased from MP Biomedicals (Irvine, CA).

Enzymes. wt RB69pol and tm RB69pol, in an exonuclease-deficient background (D222A and D327A), were overexpressed in *Escherichia coli* strain BL21(DE), purified, and stored as previously described.[36] Phi29pol (exo$^-$) was overexpressed in *E. coli* strain BL21(DE) and purified as previously described.[37]

DNA Substrates. Oligonucleotides were synthesized at the Keck facilities (Yale University). The sequences of the primer−template (P/T) used in this study were 5′-GCGGACTGCT-TAY (primer) and 5′-TCA**X**ZTAAGCAGTCCGCG, where X is THF, Y is C, G, A, or T, and Z is G, C, T, or A for Y−Z Watson−Crick base pairs. For kinetic studies, the primer was labeled at the 5′-end with ^{32}P using T4 polynucleotide kinase and [γ-^{32}P]ATP and annealed to unlabeled templates by being heated to 95 °C and then slowly cooled to 25 °C to give fully duplexed P/Ts. For crystallization, Y is ddC, ddG, ddA, or ddT to prevent phosphoryl transfer.

Chemical Quench Experiments. Rapid chemical quench experiments were performed at 23 °C with a buffer solution containing 66 mM Tris-HCl (pH 7.4) and 10 mM $MgSO_4$ using a KinTek RFQ-3 instrument (KinTek Corp., University Park, PA). Experiments were performed under single-turnover conditions, with a 10-fold excess of RB69pol over the P/T. The final concentrations after mixing were 1 μM enzyme, 83 nM ^{32}P-labeled P/T, and 10 mM Mg^{2+}. Reactions were quenched with 0.5 M EDTA (pH 8.0). Substrates and products were separated by 19:1% (w/v) PAGE containing 8 M urea, visualized using a MD Strom 860 imager (Molecular Imaging), and quantified using ImageQuaNT. For each K_d and k_{pol} determination, seven different dNTP concentrations were used. The amount of product formed versus time was plotted for each dNTP concentration and fit by nonlinear regression to the equation [product] = $A[1 - \exp(-k_{obs}t)]$, where A is the observed amplitude of product formation and k_{obs} is the observed rate constant. The kinetic parameters k_{pol} (the maximal rate of dNMP incorporation) and $K_{d,app}$ (defined as the dNTP concentration at which the rate of dNMP incorporation reaches $^1/_2k_{pol}$) were obtained by plotting k_{obs} versus [dNTP] to a hyperbolic equation: $k_{obs} = (k_{pol}[dNTP])/(K_d + [dNTP])$, where k_{obs} represents the observed rate at a given [dNTP].

Crystallization of dNTP/THF-Containing tm RB69pol Ternary Complexes. Dideoxy-terminated oligos were used for crystallization. The tm RB69pol (final concentration of 110 μM) was mixed with an equimolar ratio of freshly annealed duplex DNA. A solution of dNTP was then added to give a final concentration of 2 mM. The complex containing dGTP was prepared using the soaking replacement method from the preformed dCTP-containing crystals. Crystals were grown under oil using a microbatch procedure.[38] A solution of 100 mM $CaCl_2$, 15% (w/v) PEG 350 monomethyl ether (MME), and 100 mM sodium cacodylate (pH 6.5) was mixed with an equal volume of the protein complex. The rectangular-shaped crystals typically grew in 2 days at 20 °C and had dimensions of ~0.1 mm × ~0.1 mm × ~0.2 mm. Crystals were transferred from the mother liquor to a cryoprotectant solution containing 30% (w/v) PEG 350 MME, 100 mM $CaCl_2$, and 100 mM

dx.doi.org/10.1021/bi300296q | *Biochemistry* 2012, 51, 4922−4931

Table 1. Crystallographic Statistics for Data Collection and Structure Refinement of dNTP/THF-Containing Ternary Complexes Formed by tm RB69pol with ddC/dG as the PBP[a]

	dATP vs THF (triple mutant)	dCTP vs THF (triple mutant)	dGTP vs THF (triple mutant)	dTTP vs THF (triple mutant)
space group	$P2_12_12_1$	$P2_12_12_1$	$P2_12_12_1$	$P2_12_12_1$
unit cell [a, b, c (Å)]	75.0, 120.1, 130.5	75.0, 120.1, 130.7	74.9, 120.0, 130.6	75.4, 120.2, 131.6
resolution (Å)	50.0−2.04	50.0−1.96	50.0−1.87	50.0−1.84
no. of unique reflections	75390	107757	97840	100249
redundancy	4.7 (3.4)	4.7 (4.0)	4.7 (3.1)	4.4 (2.9)
completeness (%)	99.3 (96.2)	98.3 (90.4)	99.3 (92.4)	97.1 (80.2)
R_{merge}[b] (%)	10.1 (98.6)	4.5 (14)	7.8 (80.7)	6.4 (65.5)
I/σ	11.8 (1.0)	27.6 (10.9)	16.0 (1.2)	19.4 (1.5)
final model				
no. of amino acid residues	903	903	903	903
no. of water molecules	610	883	798	795
no. of Ca^{2+} ions	4	4	6	4
no. of template nucleotides	18	18	18	18
no. of primer nucleotides	13	13	13	13
no. of dNTPs	1	1	1	1
Refinement				
no. of reflections	71342	79816	92567	94921
R[c] (%)	18.1 (27.3)	16.7 (16.8)	17.1 (27.3)	17.2 (26.6)
R_{free} (%)	22.8 (33.7)	20.8 (22.4)	20.2 (29.4)	20.5 (30.6)
rmsd[d]				
bond lengths (Å)	0.009	0.008	0.008	0.008
bond angles (deg)	1.187	1.112	1.089	1.102
PDB entry	4DTR	4DTS	4DTU	4DTX

[a]Statistics for the highest-resolution shell are given in parentheses. [b]$R_{merge} = \sum_{hkl}\sum_j|I_j(hkl) - \langle I(hkl)\rangle|/\sum_{hkl}\langle I(hkl)\rangle$ (statistics for merging all observations for given reflections). [c]$R = \sum_{hkl}|F_{obs}(hkl) - F_{calc}(hkl)|/\sum_{hkl}F_{obs}(hkl)$ (statistics for crystallographic agreement between the measured and model-calculated amplitudes). R_{free} is the agreement for the cross-validation data set. [d]Root-mean-square deviation from ideal values.

sodium cacodylate (pH 6.5) prior to being frozen in liquid nitrogen.

Data Collection, Structure Determination, and Refinement. X-ray diffraction data were collected at 110 K, using synchrotron radiation sources at beamline 24ID-E [Northeast Collaborative Access Team (NECAT), Advanced Photon Source (APS), Argonne National Laboratory (ANL), Chicago, IL]. The data were processed using the HKL2000 program suite (Tables 1 and 2). The structures were determined by molecular replacement using Phaser,[39] starting with the pol structure from the ternary complex of wt RB69pol from Protein Data Bank (PDB) entry 3NCI,[35] and refined using REFMAC5.[40] The P/T duplex and dNTP were built into electron density maps using COOT.[41] Structure refinement statistics are summarized in Tables 1 and 2. Figures were created with Pymol.[42]

PDB Entries. Coordinates and structure factors for the THF-containing tm RB69pol ternary complex structure have been deposited in the Protein Data Bank as entries 4DTR, 4DTS, 4DTU, 4DTX, 4DTJ, 4DTM, 4DTN, 4DTO, and 4DTP.

RESULTS AND DISCUSSION

Kinetic Parameters for Incorporation of dNMPs opposite THF with dC/dG at the PBP by the wt and tm RB69pols. We have determined pre-steady-state kinetic parameters for incorporation of each of the four dNMPs opposite an abasic (THF) site with dC/dG at the PBP catalyzed by the wt and tm RB69pols. The order of incorporation efficiencies (k_{pol}/K_d) catalyzed by wt RB69pols, listed in Table 3, is consistent with the generally accepted A rule, namely that DNA polymerases preferentially insert dAMP opposite an abasic site. Similarly, the order of k_{pol}/K_d values exhibited by the tm RB69pol follows the same pattern that is seen with wt RB69pol, but the differences in incorporation among the incoming dNTPs are greatly decreased (Table 3). There is a 280-fold difference in incorporation efficiency between an incoming dATP compared to dCTP when opposite THF with wt RB69pol. In contrast, an only 18-fold difference in incorporation efficiency was observed between dAMP and dCMP opposite THF with the tm RB69pol (Table 3). Clearly, the tm RB69pol reduced the A rule selection gap by 15-fold relative to that of wt RB69pol. This change appears to be due to elimination of the rigid hydrogen bonding network present in the NBP of wt RB69pol, so that the tm RB69pol has increased flexibility in the NBP.[38,43] In addition, it is interesting that the tm RB69pol incorporates dAMP and dGMP opposite an abasic site with almost equal efficiency, deviating from the classic A rule.

Kinetic Parameters for Incorporation of dNMPs opposite THF by the tm and wt RB69pol with Various PBs. To determine the effect of different PBs on the incorporation efficiency of an incoming dNTP, we determined the pre-steady-state kinetic parameters for incorporation of each of the four dNTPs opposite an abasic site by tm RB69pol with all 16 possible PB combinations (Table 4). We were surprised to find that there was a nearly 210-fold difference in incorporation efficiency depending on the identities of the incoming dNTPs and the PBs. The highest incorporation efficiency (1.47 μM^{-1} s^{-1}) was observed when the PB was dC/dG and the incoming dNTP was dATP. The lowest incorporation efficiency (0.007 μM^{-1} s^{-1}) was observed when

dx.doi.org/10.1021/bi300296q | Biochemistry 2012, 51, 4922−4931

Table 2. Crystallographic Statistics for Data Collection and Structure Refinement of dNTP/THF-Containing Ternary Complexes Formed by tm RB69pol with Different PBs[a]

	ddT/dA/dTTP	ddG/dC/dCTP	ddA/dT/dATP	ddA/dT/dCTP	ddA/dT/dGTP
PB	ddT/dA	ddG/dC	ddA/dT	ddA/dT	ddA/dT
dNTP	dTTP	dCTP	dATP	dCTP	dGTP
space group	$P2_12_12_1$	$P2_12_12_1$	$P2_12_12_1$	$P2_12_12_1$	$P2_12_12_1$
unit cell [*a*, *b*, *c* (Å)]	75.1, 119.8, 130.5	75.2, 120.5, 130.8	78.3, 118.1, 130.2	78.2, 119.3, 130.9	78.5, 118.3, 130.7
resolution (Å)	50.0−1.90	50.0−1.95	50.0−1.96	50.0−2.05	50.0−2.04
no. of unique reflections	92548	86912	86518	78651	75856
redundancy	3.6 (3.4)	3.6 (3.7)	3.9 (3.9)	3.6 (3.7)	3.6 (3.6)
completeness (%)	99.1 (99.0)	99.6 (99.9)	99.7 (100.0)	99.5 (100.0)	99.2 (99.9)
R_{merge}[b] (%)	6.0 (24.5)	9.2 (74.4)	9.8 (83.2)	8.7 (70.6)	11.4 (71.5)
I/σ	18.7 (4.0)	12.8 (1.3)	12.5 (1.3)	12.9 (1.3)	10.7 (1.6)
final model					
no. of amino acid residues	903	903	903	903	903
no. of water molecules	906	700	645	562	597
no. of Ca^{2+} ions	5	5	5	5	5
no. of template nucleotides	18	18	18	18	18
no. of primer nucleotides	13	13	13	13	13
no. of dNTPs	1	1	1	1	1
Refinement					
no. of reflections	87843	82442	82125	74651	71956
R[c] (%)	17.1 (21.4)	18.4 (30.5)	18.4 (27.6)	18.4 (27.1)	18.9 (25.4)
R_{free} (%)	20.2 (25.4)	22.0 (36.2)	21.6 (32.4)	22.5 (32.6)	22.9 (30.3)
rmsd[d]					
bond lengths (Å)	0.006	0.006	0.006	0.006	0.006
bond angles (deg)	1.106	1.085	1.050	1.078	1.112
PDB entry	4DTJ	4DTM	4DTN	4DTO	4DTP

[a]Statistics for the highest-resolution shell are given in parentheses. [b]$R_{merge} = \sum_{hkl}\sum_j|I_j(hkl) - \langle I(hkl)\rangle|/\sum_{hkl}\langle I(hkl)\rangle$ (statistics for merging all observations for given reflections). [c]$R = \sum_{hkl}|F_{obs}(hkl) - F_{calc}(hkl)|/\sum_{hkl}F_{obs}(hkl)$ (statistics for crystallographic agreement between the measured and model-calculated amplitudes). R_{free} is the agreement for the cross-validation data set. [d]Root-mean-square deviation from ideal values.

Table 3. Pre-Steady-State Kinetic Parameters for Incorporation of dNTPs opposite THF by wt and tm RB69pol When dC/dG Is in the PBP[a]

pol	dNTP/THF	k_{pol} (s^{-1})	K_d (μM)	k_{pol}/K_d (μM^{-1} s^{-1})	ratio[b]
wt	dATP/THF	0.30 ± 0.01	1400 ± 100	2.1×10^{-4}	313
wt	dGTP/THF	0.17 ± 0.01	1800 ± 200	9.4×10^{-5}	140
wt	dTTP/THF	NAD[c]	NAD[c]	2.7×10^{-6}	4
wt	dCTP/THF	NAD[c]	NAD[c]	6.7×10^{-7}	1
tm	dATP/THF	360 ± 9	250 ± 24	1.44	18
tm	dGTP/THF	240 ± 12	170 ± 30	1.41	17
tm	dTTP/THF	210 ± 14	830 ± 140	0.25	3
tm	dCTP/THF	150 ± 10	1900 ± 250	0.08	1

[a]The corresponding progress curves and plots of k_{obs} vs [dNTP] are shown in Figures S1 and S2 of the Supporting Information. [b]Incorporation efficiency ratio relative to the lowest value for each enzyme. [c]Not accurately determined. The resulting k_{pol}/K_d value is either from an extrapolation of data fitting or from the slope of the plot of k_{obs} vs [dNTP].

the PB was dA/dT and the incoming dNTP was dCTP. These results suggest that there are specific interactions between the base of incoming dNTPs and the PB. The influence of PB's identity on incorporation efficiency was not known or obvious from previous kinetic and structural data when incoming dNTPs were opposite complementary templating nucleotide residues as no significant differences were observed with either the tm RB69pol or the wt enzyme.[32]

For a given incoming dNTP, the difference in incorporation efficiency varies from 11-fold (when the incoming dNTP is dATP) to 41-fold (when the incoming dNTP is dCTP) (Table 4). From these results, it is clear that interactions other than base stacking between the incoming dNTP and the PB must be involved. Analysis of these kinetic variations revealed the following pattern: (i) For a given PB, dAMP is always incorporated more efficiently than the other three dNMPs (the A rule); (ii) For a given incoming dNTP, the incorporation efficiency when the PB is dC/dG or dG/dC is higher than when the PB is dA/dT or dT/dA. This is consistent with the fact that there is more "breathing" in duplex DNA that has A/T rich sequences at the P/T junction; (iii) For purine dNTPs (dPuNTPs), the incorporation efficiency is the highest when the PB is dC/dG and is lowest when the PB is dA/dT (Table 4).

To see if the same pattern would hold for wt RB69pol, we determined corresponding kinetic parameters for incorporation of dCTP and dTTP opposite an abasic site with eight possible PB combinations. When dTTP is the incoming dNTP, the incorporation efficiency is the highest when the PB is dC/dG and is lowest when the PB is dT/dA (Table 5). This trend is

dx.doi.org/10.1021/bi300296q | Biochemistry 2012, 51, 4922−4931

Table 4. Pre-Steady-State Kinetic Parameters for Incorporation of dNTPs opposite THF by the tm RB69pol with Different Penultimate Base Pairs[a]

penultimate BP[b]	incoming dNTP	k_{pol} (s^{-1})	K_d (μM)	k_{pol}/K_d (μM^{-1} s^{-1})	ratio[c]
dG/dC	dCTP	170 ± 5	590 ± 50	0.29	41
dC/dG		150 ± 10	1900 ± 250	0.08	11
dT/dA		NAD	NAD	0.015	2
dA/dT		NAD	NAD	0.007	1
dC/dG	dTTP	210 ± 14	830 ± 140	0.25	31
dG/dC		NAD	NAD	0.04	5
dA/dT		NAD	NAD	0.01	1
dT/dA		NAD	NAD	0.008	1
dC/dG	dATP	360 ± 9	250 ± 24	1.44	11
dG/dC		120 ± 2	150 ± 13	0.80	6
dT/dA		130 ± 7	380 ± 80	0.34	3
dA/dT		150 ± 6	1100 ± 130	0.13	1
dC/dG	dGTP	240 ± 12	170 ± 30	1.41	35
dG/dC		230 ± 6	660 ± 60	0.35	9
dT/dA		120 ± 7	1100 ± 210	0.10	3
dA/dT		NAD	NAD	0.04	1

[a]NAD stands for not accurately determined. The resulting k_{pol}/K_d value is either from an extrapolation of data fitting or from the slope of the plot of k_{obs} vs [dNTP]. The corresponding progress curves and plots of k_{obs} vs [dNTP] are shown in Figures S3 and S4 of the Supporting Information. [b]With the penultimate BP, the base in the primer strand is shown on the left and the base in the template strand is shown on the right. [c]Incorporation efficiency ratio relative to the lowest value for each dNTP.

Table 5. Pre-Steady-State Kinetic Parameters for Incorporation of dNTPs opposite THF by the wt RB69pol with Different Penultimate Base Pairs

penultimate BP[b]	incoming dNTP	k_{pol}/K_d (μM^{-1} s^{-1})[a]	ratio[b]
dC/dG	dCTP	6.7×10^{-7}	7
dA/dT		3.6×10^{-7}	4
dG/dC		3.3×10^{-7}	3
dT/dA		1.0×10^{-7}	1
dC/dG	dTTP	2.7×10^{-6}	9
dG/dC		1.2×10^{-6}	4
dA/dT		1.2×10^{-6}	4
dT/dA		3.3×10^{-7}	1

[a]The k_{pol}/K_d value was calculated by using $k_{pol}/[dNTP]_{sub}$, where [dNTP] = 5 mM. The k_{pol}/K_d values for dC/dG with incoming dCTP and dTTP were taken from Table 1. [b]Incorporation efficiency ratio relative to the lowest value for each dNTP.

consistent with that found with the tm RB69pol. However, when dCTP is the incoming dNTP, the order of incorporation efficiency with four possible PB combinations follows a different pattern compared to that observed with the tm RB69pol (Tables 4 and 5). It is important to note that the ratio of differences between the highest and lowest efficiency of incorporation for each dNTP by the wt enzyme is 3−6-fold less than that found with the mutant. Therefore, certain interactions between the incoming dNTP and the PB must be amplified in the presence of tm RB69pol.

Kinetic Parameters for Incorporation of dAMP opposite dT when Bypassing a dN/THF Lesion. Unlike other DNA pols, the wt RB69pol inserts dGMP opposite an abasic site (THF) almost as efficiently as dAMP with only a 2-fold difference, which is insignificant with respect to the A rule selection. With the tm RB69pol, dAMP and dGMP are incorporated opposite an abasic site with equal efficiency (violating the classic A rule, Table 3). To further investigate the extent to which the tm RB69pol was more permissive than the wt RB69pol, we determined the pre-steady-state kinetic parameters for incorporation of dAMP opposite dT when bypassing a dN/THF lesion catalyzed by the tm RB69pol (Table 6). Interestingly, the tm RB69pol was able to bypass a

Table 6. Pre-Steady-State Kinetic Parameters for Incorporation of dATP opposite dT Bypassing a dN/THF Lesion by the wt and tm RB69pol

pol	bypass dN/THF	k_{pol}/K_d (μM^{-1} s^{-1})[a]	ratio[b]
tm RB69pol	dA/THF	7.9×10^{-5}	98
tm RB69pol	dG/THF	6.4×10^{-6}	8
tm RB69pol	dT/THF	1.8×10^{-6}	2
tm RB69pol	dC/THF	8.0×10^{-7}	1
wt RB69pol	dA/THF	1.0×10^{-6}	24
wt RB69pol	dG/THF	5.6×10^{-8}	1
wt RB69pol	dC/THF	4.8×10^{-8}	1
wt RB69pol	dT/THF	4.2×10^{-8}	1
Phi29pol	dA/THF	9.0×10^{-7}	45
Phi29pol	dG/THF	4.4×10^{-8}	2
Phi29pol	dC/THF	2.7×10^{-8}	1
Phi29pol	dT/THF	2.0×10^{-8}	1

[a]The k_{pol}/K_d values for wt RB69pol and Phi29pol were calculated by using $k_{pol}/[dNTP]_{sub}$, where [dNTP] = 5 mM. The corresponding progress curves and plots of k_{obs} vs [dNTP] by tm RB69pol are shown in Figure S5 of the Supporting Information. [b]Incorporation efficiency ratio relative to the lowest value for each enzyme.

dA/THF lesion 14-fold more efficiently than a dG/THF site, 49-fold more efficiently than a dT/THF site, and almost 100-fold more efficiently than a dC/THF lesion. As shown in Table 6, the same trend was also observed for wt RB69pol and Phi29pol, another B family pol. This trend is more important for burying the abasic site to allow for uninterrupted DNA replication. On the basis of these results, we propose that the A rule can be extended, namely that B family polymerases can bypass dA/THF sites much more efficiently than other dN/THF lesions.

Overview of Crystal Structures of tm RB69pol Ternary Complexes Containing Each of the Four dNTPs opposite an Abasic Site. In our initial structural studies, a standard P/T

dx.doi.org/10.1021/bi300296q | Biochemistry 2012, 51, 4922−4931

was used in which the PB was ddC/dG.[44] With this P/T, we have obtained four crystal structures of tm RB69pol ternary complexes containing an abasic site opposite each of the four incoming dNTPs at resolutions varying from 1.84 to 2.04 Å (Table 1). These structures have been refined with cross-validation *R* factors varying from 20.2 to 22.8%. Following kinetic studies with different PBs, we have determined five additional structures of tm RB69pol complexes containing an abasic site in the DNA substrate, again opposite each of the four incoming dNTPs. These five new ternary complexes were chosen to represent ones displaying the highest and lowest incorporation efficiencies for each incoming dNTP and were determined at resolutions varying from 1.9 to 2.0 Å with free *R* factors varying from 20.2 to 22.9% (Table 2). The overall structures of all nine ternary complexes containing an abasic site are identical to that of the dCTP/dG-containing wt RB69pol ternary complex. The root-mean-squared deviation for Cα atoms between the highest-resolution ternary complex structure of the tm RB69pol (containing dTTP/THF, 1.8 Å) and the wt RB69pol (containing dCTP/dG, 1.8 Å) is 0.12 Å, which suggested that the three amino acid substitutions in the NBP of tm RB69pol did not alter the overall structure. In all cases, the electron densities for P/Ts containing a templating THF, the incoming dNTP, and the surrounding network of ordered water molecules were well-defined (Figure 2).

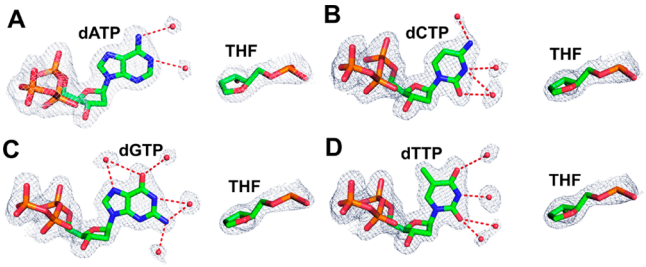

Figure 2. Structures of the dNTP/THF nascent base pairs in the ternary complexes of tm RB69pol with ddC/dG at the PBP superimposed onto the final $2F_o - F_c$ electron density maps contoured at 1.2σ. (A) dATP/THF structure at 2.04 Å resolution. (B) dCTP/THF structure at 1.96 Å resolution. (C) dGTP/THF structure at 1.87 Å resolution. (D) dTTP/THF structure at 1.84 Å resolution.

Structural Basis for the Differences in Incorporation Efficiences of Purine versus Pyrimidine dNMPs opposite an Abasic Site. Our kinetic data have shown that the catalytic efficiency for incorporating purine dNTPs (dPuTP) opposite an abasic site by tm RB69pol is 7−18-fold higher than that of pyrimidine dNTPs (dPyTP). In addition, the tm RB69pol incorporates dGMP as efficiently as dAMP opposite an abasic site. These kinetic observations are consistent with the corresponding structures. Thus, in all four dNTP/THF ternary complexes, with ddC/dG at the PBP, the base of the incoming dNTP is completely stacked onto the PB. Superposition of the Cα coordinates of all four dNTP/THF structures shows that the triphosphate tail and the ribosyl moiety of the dNTPs interact with the pol in an identical manner (Figure 3A). Because dPuTPs are able to stack better against PBs in ternary complexes than dPyTPs, this could be one reason why dPuTPs are incorporated more efficiently than dPyTPs opposite an abasic site. Among the two dPuTPs, the base of dATP overlaps almost completely with that of dGTP when the two complexes are superimposed (Figure 3A). Both dPuTPs stack equally well

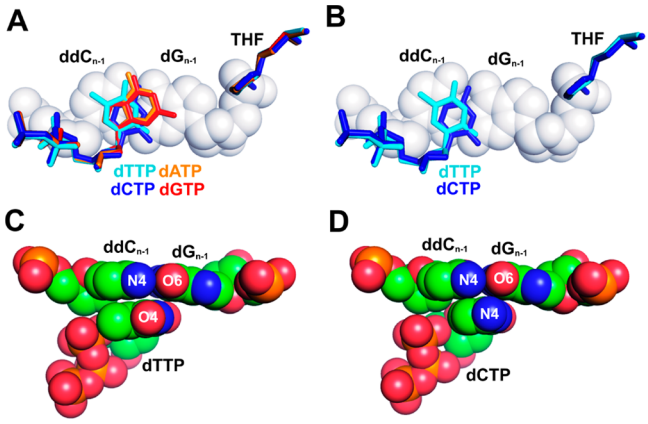

Figure 3. Geometry of base stacking and partial charge interactions with fixed PB's dCTP/dG. (A) Superposition of tm RB69pol Cα coordinates of the four complexes (dATP/THF, orange; dCTP/THF, blue; dGTP/THF, red; dTTP/THF, cyan). The PB's ddC/dG is shown as a space filling model. (B) Superposition of tm RB69pol Cα coordinates of the two pyrimidine/THF-containing complexes (dCTP/THF, blue; dTTP/THF, cyan). (C) dTTP and the PB's ddC/dG in the dTTP/THF-containing tm RB69pol. (D) dCTP and the PB's ddC/dG in the dCTP/THF-containing tm RB69pol.

against the PB and could account for the fact that the tm RB69pol incorporates both dPuTPs with equal efficiency. Between the two dPyTPs, the base of dTTP is tilted more toward its triphosphate tail compared to dCTP (Figure 3B). The interatomic distance between the C6 and O5′ atoms of the incoming dTTP is 3.27 Å, and the corresponding distance for the incoming dCTP is 3.54 Å. As a result, the base of dTTP stacks right on top of ddC, which is the 3′-terminal base in the primer strand of the PB, and the partial negatively charged O4 of dTTP lies exactly over the partial positively charged N4 of ddC (Figure 3C). In contrast, the base of dCTP stacks on top of the surface of the ddC/dG pair near its base pairing interface at the primer−template junction, and N4 of dCTP is equidistant from N4 of ddC and O6 of dG (Figure 3D). Therefore, better π−π stacking between the dTTP and ddC together with interactions of the complementary partial charges between O4 of dTTP and N4 of ddC could explain why the tm RB69pol incorporates dTTP 3-fold more efficiently than dCTP when opposite an abasic site.

Because of the smaller stacking surface of pyrimidines compared to that of purines, we suspect that the partial charge interactions between the base of the incoming dNTP and the base in the primer strand at the PBP would have a more significant effect on the insertion efficiency of dPyTPs than on that of dPuTPs. This speculation is consistent with what we have observed in structures with different PBs. The incorporation efficiency of dCMP opposite an abasic site is highest when the PB is dG/dC (0.29 μM^{-1} s^{-1}) and lowest when the PB is dA/dT (0.007 μM^{-1} s^{-1}). As shown in Figure 4A, the partial positively charged N4 of dCTP lies on top of the partial negatively charged O6 of ddG, and the partial negatively charged O2 of dCTP is situated right over the partial positively charged N2 of ddG. The positive and negative partial charge interactions of these four atoms help to stabilize the ternary complex. In contrast, the partial positively charged N4 of dCTP is positioned just adjacent to the partial positively charged N6 of ddA in the dCTP-containing structure with ddA/dT at the PBP (Figure 4B). The resulting repulsive interactions would likely destabilize the ternary complex. Therefore, the differences

dx.doi.org/10.1021/bi300296q | *Biochemistry* 2012, 51, 4922−4931

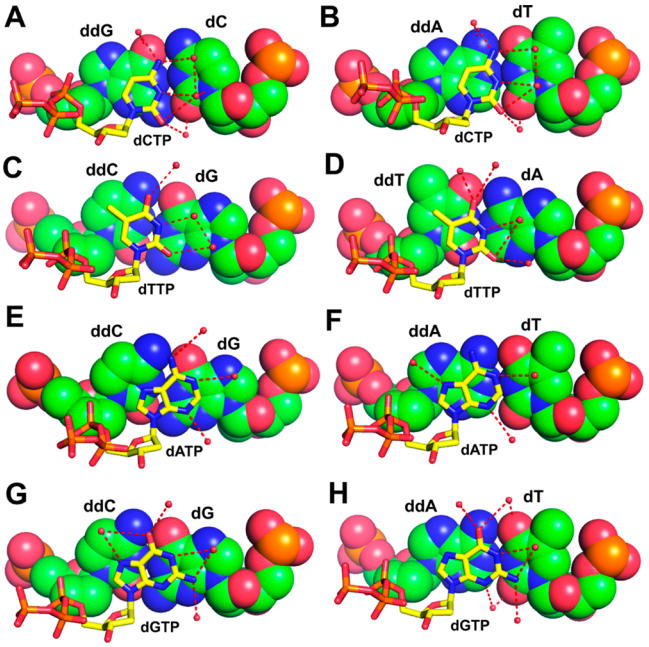

Figure 4. Base stacking of the incoming dNTP with different PBs. The incoming dNTP is shown as thick sticks, and the PB is shown as a space filling model. (A) dCTP with ddG/dC. (B) dCTP with ddA/dT. (C) dTTP with ddA/dT. (D) dTTP with ddT/dA. (E) dATP with ddC/dG. (F) dATP with ddA/dT. (G) dGTP with ddC/dG. (H) dGTP with ddA/dT.

in partial charge interactions between dCTP and the PBs are likely to account for the 41-fold difference in catalytic efficiency for dCMP incorporation in these two contexts. The same phenomena were observed when the incoming dNTP was dTTP. The incorporation efficiency of dTMP opposite an abasic site is highest when the PB is dC/dG (0.26 μM^{-1} s^{-1}) and lowest when the PB is dT/dA (0.013 μM^{-1} s^{-1}) (Table 4). In the ternary structure with ddC/dG at the PBP, the partial negatively charged O4 and O2 of dTTP stack neatly on the surface of the partial positively charged N4 of ddC and N2 of dG, respectively (Figure 4C). In contrast, the partial negatively charged O4 of dTTP stacks right over the partial negatively charged O4 of ddT in the structure where ddT/dA is at the PBP (Figure 4D).

When the incoming dNTP is a dPuTP, its efficiency of incorporation opposite an abasic site is highest when the PB is ddC/dG and lowest when the PB is dA/dT. As shown in panels E and G of Figure 4, both N6 of dATP and O6 of dGTP are positioned just over the interface of the ddC/dG pair at the primer–template junction. When the PB is ddA/dT, the partial positively charged N6 of dATP stacks on the surface of the partial positively charged N6 of ddA (Figure 4F), and the partial negatively charged O6 of dGTP stacks on top of the partial positively charged N6 of ddA (Figure 4H). Therefore, partial charge interactions between the dNTPs and the PBs are not likely to be the major factors influencing the efficiencies of incoporation of dPuTPs opposite an abasic site. Upon examination of all the THF-containing structures, a common feature is that the bases of the incoming dNTPs remain partially hydrated in the NBP (Figures 2 and 4). Nearly all HB donors and acceptors of dNTPs have at least one ordered water molecule within HB distance. These ordered water molecules are located on the PB surface as part of an ordered hydration network. Thus, without a templating base, the incoming dNTP failed to dehydrate its W–C base pairing face when forming a ternary complex relative to the ternary complex with a W–C templating base. When the PB is ddA/dT and the incoming dNTP is a dPuTP, the ordered water molecules are located just over the C atoms of the PB. Such hydration of incoming dNTPs would be expected to destabilize the ternary complex. In contrast, when the PB is ddC/dG, the ordered water molecules are located very close to the N atoms of the dG base. Given this proximity, these ordered water molecules would be expected to help stabilize the ternary complex. Therefore, the extent of hydration around the incoming base and PBP is likely to be a key determinant for the observed kinetic variations with respect to incoming dPuTPs (Table 3).

We have not been able to obtain crystals of the ternary complex of wt RB69pol with THF at the n position of the template strand because of the high apparent dissociation constant. Our previous structural studies with the dGTP/dC-containing wt RB69pol have shown that there is a rigid HB network in the minor groove of the nascent P/T duplex. This network includes five ordered water molecules and the side chain hydroxyl groups of Y567, Y416, and T622. Also, Y567 forms a HB with the O2 or N3 atom of PB at the template strand via a water molecule. In contrast, the Y567 to Ala substitution in the tm RB69pol disrupted this rigid HB network and the space generated by removing the hydroxyphenyl group of Y567 is occupied by additional water molecules that are no longer within HB distance of the O2 or N3 atom of PB. Therefore, the charge distribution around the exocyclic groups of the PB might be slightly different between the wt pol and tm pol. Together with the flexibility of NBP in the tm RB69pol, the partial charge interactions between the PB and the incoming dNTP might somehow be amplified in the context of the tm pol. That might be the reason why the difference in incorporation efficiency with different PBs for each dNTP by the wt enzyme is 3–6-fold less than that of the mutant, although we cannot rule out other possibilities without the structure of the dNTP/THF-containing ternary complex of wt RB69pol.

Structural Comparison of THF-Containing Ternary Complexes with DNA Polymerases from Other Families. Studies of replication past abasic lesions in DNA have been conducted extensively with DNA polymerases from several families, and it is clear that different mechanisms are used by the various pols to bypass abasic sites.[16,22,23,26,45,46] In addition to the structures reported in this study, structures of DNA polymerases from families A, B, X, and Y bound to THF-containing duplex DNA are available.[22]

As a representative of the A family polymerases, KlenTaq, the large fragment of *Thermus aquaticus* DNA polymerase I, follows the A rule by utilizing an amino acid templating mechanism. As shown in Figure 5A, Y671, a highly conserved residue in the A family DNA pols, forms a hydrogen bond with N3 of the incoming dATP. This interaction facilitates nucleotide incorporation by mimicking a pyrimidine nucleobase for directing incorporation of dAMP opposite an abasic site.[23] R283 of pol β, a family X polymerase, is another example in which an amino acid residue directs the incorporation of dAMP opposite THF.[8] In this case, R283 was observed to make a hydrogen bond with the THF phosphate backbone (Figure 5B). It was proposed that misinsertion may occur through a similar "abasic site intermediate". In contrast to KlenTaq and pol β, Dpo4, a family Y polymerase, can efficiently replicate DNA past an abasic lesion by looping out the abasic site.[47] As

dx.doi.org/10.1021/bi300296q | *Biochemistry* 2012, 51, 4922–4931

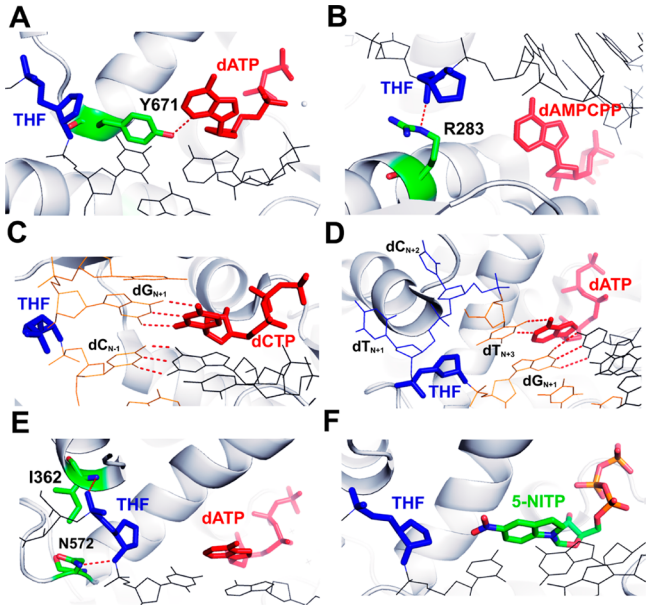

Figure 5. Structural comparison with other known THF-containing ternary complexes. (A) NBP of the dATP/THF-containing ternary complex of KlenTaq. (B) NBP of the dAMPCPP/THF-containing ternary complex of pol *β*. (C) NBP of the dCTP/THF-containing ternary complex of Dpo4. (D) NBP of the dATP/THF-containing ternary complex of PolII. (E) NBP of the dATP/THF-containing ternary complex of tm RB69pol. (F) NBP of the 5-NITP/THF-containing ternary complex of wt RB69pol. The incoming dNTP is colored red; the THF moiety is colored blue, and the protein residues are colored green. The polymerase is shown as a gray cartoon.

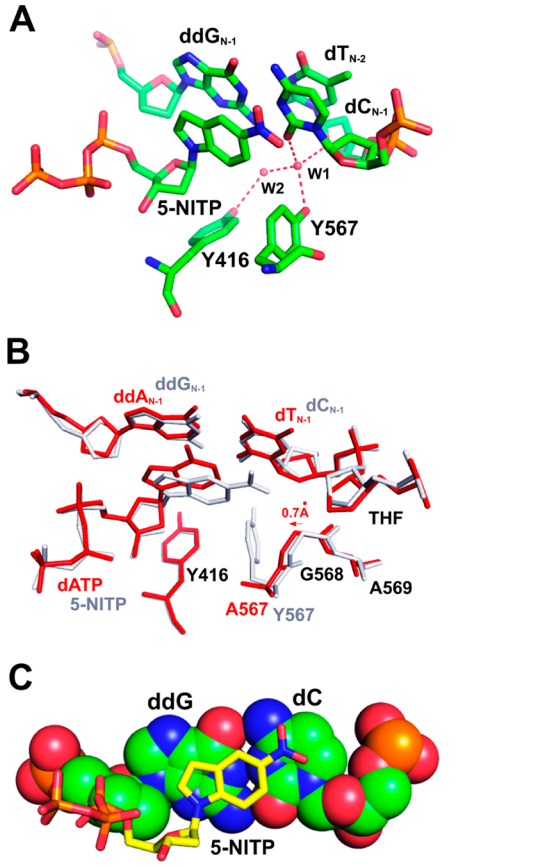

Figure 6. Structural comparison of the THF-containing ternary complexes of wt and tm RB69pols. (A) HB network in the NBP of the 5-NITP/THF-containing ternary complex of wt RB69pol. (B) Superposition of C*α* coordinates of the dATP/THF-containing ternary complex of tm RB69pol (red sticks) with the 5-NITP/THF-containing ternary complex of wt RB69pol (white sticks). (C) Base stacking of the incoming 5-NITP (yellow) with the PB (space filling model).

shown in Figure 5C, the abasic site remains extrahelical and the incoming dCTP pairs with a base 5′ to the lesion. Primer extension then generates a −1 frameshift.[47] *E. coli* DNA pol II, a family B polymerase, is another DNA pol that employs a looping-out mechanism. A small cavity outside the NBP of pol II can accommodate a looped-out template 2 bp upstream. As a result, the incoming dATP base pairs with dT at position $N + 3$ of the template strand (Figure 5D).[46] By contrast, in all nine structures of THF-containing ternary complexes of tm RB69pol reported here, neither insertion of a protein side chain nor looping out of the abasic site was observed. Rather, the abasic lesion in all nine ternary complexes of tm RB69pol was locked in place by two hydrogen bonds: one between N572 and a phosphate oxygen on the 3′ side of the lesion and the other between the backbone amide hydrogen of I362 and the phosphate oxygen of the lesion (Figure 5E). These two hydrogen bond interactions are probably why the abasic lesion does not loop out in RB69pol, although the overall structure of RB69pol is quite similar to that of pol II.

Zahn et al.[27] have reported a structure of the wt RB69pol ternary complex containing an abasic site paired with an unnatural purine triphosphate analogue, 5-NITP (Figure 5F). A rigid hydrogen bonding network involving the minor groove of the P/T duplex and Y567 was also observed in the 5-NITP-containing structure (Figure 6A). Least-squares superimposition of the 5-NITP-containing ternary complex of wt RB69pol with the dATP/THF-containing ternary complex of tm RB69pol shows that: (i) the bases of 5-NITP and dATP are in the same plane but the indole ring of 5-NITP tilts more toward the minor groove to maximize the stacking interaction with the ddG/dC at the PBP (Figure 6B), (ii) the A567 and G568 main chain amide linkage shifts 0.7 Å laterally toward the Y416 side chain (Figure 6B) and; (iii) the W1 water molecule was absent in the tm RB69pol complex (Figure 6A) and the rigid hydrogen bonding network was disrupted. This is consistent with the increased efficiency of incorporation for all the dNMPs opposite an abasic site (10^4−10^5-fold) exhibited by tm RB69pol relative to wt. Interestingly, a partial charge interaction between the negatively charged O5 of 5-NTIP and the positively charged N4 of dC was observed (Figure 6C). According to the explanation of Zahn et al.,[27] this partial charge interaction was probably why 5-NITP is incorporated more efficiently than dAMP opposite an abasic site and is consistent with our observation of tm RB69pol that partial charge interactions between the incoming dNTPs and the PB play a dominant role in determining the value of the corresponding kinetic parameters.

To summarize, we have shown that, in addition to base stacking, partial charge interactions between the incoming dNTP and the penultimate base pair make significant contributions to the efficiencies of incorporation of dNTPs opposite abasic sites in the context of the tm RB69pol. Although this trend might be specific to tm RB69pol, it provides the first example that partial charge interactions between the PB and incoming dNTP can modulate insertion

dx.doi.org/10.1021/bi300296q | *Biochemistry* 2012, 51, 4922−4931

efficiency. In addition, we also propose an extension of the A rule, namely that B family polymerases can bypass a dA/THF site much more efficiently than any other dN/THF pair. Taken together, the results presented here add another dimension to the extensive literature about the structural basis for bypassing abasic sites by DNA pols.

■ ASSOCIATED CONTENT

Supporting Information

Fiev additional figures. This material is available free of charge via the Internet at http://pubs.acs.org.

■ AUTHOR INFORMATION

Corresponding Author

*W.H.K.: phone, (203) 785-4599; e-mail, william.konigsberg@yale.edu. J.W.: phone, (203) 432-5737; e-mail, jimin.wang@yale.edu.

Funding

This work was supported by National Institutes of Health Grant RO1-GM063276-09 (to W.H.K.) and by SCSB-GIST (to S.H.E. and J.W.).

Notes

The authors declare no competing financial interest.

■ ACKNOWLEDGMENTS

We thank the staff of NECAT beamline 24ID-E at the Advanced Photon Source of Argonne National Laboratory.

■ ABBREVIATIONS

pol, DNA polymerase; RB69pol, bacteriophage RB69 DNA polymerase; THF, tetrahydrofuran, an abasic nucleotide residue; NBP, nascent base pair binding pocket; P/T, primer/template DNA duplex; HB, hydrogen bond; wt, wild type; tm, triple mutant that includes the L561A, S565G, and Y567A substitutions; dNTPs, 2′-deoxynucleoside 5′-triphosphates; dNMPs, 2′-deoxynucleoside 5′-monophosphates; dPuTPs, purine dNTPs; dPyTPs, pyrimidine dNTPs; PEG 350 MME, polyethylene glycol 350 monomethyl ether; 5-NITP, 5-nitro-1-indolyl-2′-deoxyriboside 5′-triphosphate; PB, penultimate base pair; PBP, penultimate base pair position.

■ REFERENCES

(1) Lindahl, T., and Nyberg, B. (1972) Rate of depurination of native deoxyribonucleic acid. *Biochemistry 11*, 3610−3618.

(2) Nakamura, J., Walker, V. E., Upton, P. B., Chiang, S. Y., Kow, Y. W., and Swenberg, J. A. (1998) Highly sensitive apurinic/apyrimidinic site assay can detect spontaneous and chemically induced depurination under physiological conditions. *Cancer Res. 58*, 222−225.

(3) Nakamura, J., and Swenberg, J. A. (1999) Endogenous apurinic/apyrimidinic sites in genomic DNA of mammalian tissues. *Cancer Res. 59*, 2522−2526.

(4) Lindahl, T. (1993) Instability and decay of the primary structure of DNA. *Nature 362*, 709−715.

(5) Seeberg, E., Eide, L., and Bjoras, M. (1995) The base excision repair pathway. *Trends Biochem. Sci. 20*, 391−397.

(6) Hatahet, Z., Zhou, M., Reha-Krantz, L. J., Ide, H., Morrical, S. W., and Wallace, S. S. (1999) In vitro selection of sequence contexts which enhance bypass of abasic sites and tetrahydrofuran by T4 DNA polymerase holoenzyme. *J. Mol. Biol. 286*, 1045−1057.

(7) Goodman, M. F. (2002) Error-prone repair DNA polymerases in prokaryotes and eukaryotes. *Annu. Rev. Biochem. 71*, 17−50.

(8) Beard, W. A., Shock, D. D., Batra, V. K., Pedersen, L. C., and Wilson, S. H. (2009) DNA polymerase β substrate specificity: Side chain modulation of the "A-rule". *J. Biol. Chem. 284*, 31680−31689.

(9) Hubscher, U., Maga, G., and Spadari, S. (2002) Eukaryotic DNA polymerases. *Annu. Rev. Biochem. 71*, 133−163.

(10) Boiteux, S., and Laval, J. (1982) Coding properties of poly(deoxycytidylic acid) templates containing uracil or apyrimidinic sites: In vitro modulation of mutagenesis by deoxyribonucleic acid repair enzymes. *Biochemistry 21*, 6746−6751.

(11) Sagher, D., and Strauss, B. (1983) Insertion of nucleotides opposite apurinic/apyrimidinic sites in deoxyribonucleic acid during in vitro synthesis: Uniqueness of adenine nucleotides. *Biochemistry 22*, 4518−4526.

(12) Loeb, L. A., and Preston, B. D. (1986) Mutagenesis by apurinic/apyrimidinic sites. *Annu. Rev. Genet. 20*, 201−230.

(13) Randall, S. K., Eritja, R., Kaplan, B. E., Petruska, J., and Goodman, M. F. (1987) Nucleotide insertion kinetics opposite abasic lesions in DNA. *J. Biol. Chem. 262*, 6864−6870.

(14) Lawrence, C. W., Borden, A., Banerjee, S. K., and LeClerc, J. E. (1990) Mutation frequency and spectrum resulting from a single abasic site in a single-stranded vector. *Nucleic Acids Res. 18*, 2153−2157.

(15) Mozzherin, D. J., Shibutani, S., Tan, C. K., Downey, K. M., and Fisher, P. A. (1997) Proliferating cell nuclear antigen promotes DNA synthesis past template lesions by mammalian DNA polymerase delta. *Proc. Natl. Acad. Sci. U.S.A. 94*, 6126−6131.

(16) Shibutani, S., Takeshita, M., and Grollman, A. P. (1997) Translesional synthesis on DNA templates containing a single abasic site. A mechanistic study of the "A rule". *J. Biol. Chem. 272*, 13916−13922.

(17) Avkin, S., Adar, S., Blander, G., and Livneh, Z. (2002) Quantitative measurement of translesion replication in human cells: Evidence for bypass of abasic sites by a replicative DNA polymerase. *Proc. Natl. Acad. Sci. U.S.A. 99*, 3764−3769.

(18) Strauss, B. S. (2002) The "A" rule revisited: Polymerases as determinants of mutational specificity. *DNA Repair 1*, 125−135.

(19) Pages, V., Johnson, R. E., Prakash, L., and Prakash, S. (2008) Mutational specificity and genetic control of replicative bypass of an abasic site in yeast. *Proc. Natl. Acad. Sci. U.S.A. 105*, 1170−1175.

(20) Schaaper, R. M., Kunkel, T. A., and Loeb, L. A. (1983) Infidelity of DNA synthesis associated with bypass of apurinic sites. *Proc. Natl. Acad. Sci. U.S.A. 80*, 487−491.

(21) Taylor, J. S. (2002) New structural and mechanistic insight into the A-rule and the instructional and non-instructional behavior of DNA photoproducts and other lesions. *Mutat. Res. 510*, 55−70.

(22) Zahn, K. E., Wallace, S. S., and Doublie, S. (2011) DNA polymerases provide a canon of strategies for translesion synthesis past oxidatively generated lesions. *Curr. Opin. Struct. Biol. 21*, 358−369.

(23) Sale, J. E., Lehmann, A. R., and Woodgate, R. (2012) Y-family DNA polymerases and their role in tolerance of cellular DNA damage. *Nat. Rev. Mol. Cell Biol. 13*, 141−152.

(24) Fiala, K. A., Hypes, C. D., and Suo, Z. (2007) Mechanism of abasic lesion bypass catalyzed by a Y-family DNA polymerase. *J. Biol. Chem. 282*, 8188−8198.

(25) Obeid, S., Blatter, N., Kranaster, R., Schnur, A., Diederichs, K., Welte, W., and Marx, A. (2010) Replication through an abasic DNA lesion: Structural basis for adenine selectivity. *EMBO J. 29*, 1738−1747.

(26) Reineks, E. Z., and Berdis, A. J. (2004) Evaluating the contribution of base stacking during translesion DNA replication. *Biochemistry 43*, 393−404.

(27) Zahn, K. E., Belrhali, H., Wallace, S. S., and Doublie, S. (2007) Caught bending the A-rule: Crystal structures of translesion DNA synthesis with a non-natural nucleotide. *Biochemistry 46*, 10551−10561.

(28) Greenberg, M. M., Weledji, Y. N., Kroeger, K. M., and Kim, J. (2004) In vitro replication and repair of DNA containing a C2′-oxidized abasic site. *Biochemistry 43*, 15217−15222.

(29) Zhang, H., Rhee, C., Bebenek, A., Drake, J. W., Wang, J., and Konigsberg, W. (2006) The L561A substitution in the nascent base-pair binding pocket of RB69 DNA polymerase reduces base discrimination. *Biochemistry 45*, 2211−2220.

(30) Sheriff, A., Motea, E., Lee, I., and Berdis, A. J. (2008) Mechanism and dynamics of translesion DNA synthesis catalyzed by the *Escherichia coli* Klenow fragment. *Biochemistry 47*, 8527−8537.
(31) Sabouri, N., and Johansson, E. (2009) Translesion synthesis of abasic sites by yeast DNA polymerase ε. *J. Biol. Chem. 284*, 31555−31563.
(32) Zhang, H., Beckman, J., Wang, J., and Konigsberg, W. (2009) RB69 DNA polymerase mutants with expanded nascent base-pair-binding pockets are highly efficient but have reduced base selectivity. *Biochemistry 48*, 6940−6950.
(33) Berdis, A. J. (2001) Dynamics of translesion DNA synthesis catalyzed by the bacteriophage T4 exonuclease-deficient DNA polymerase. *Biochemistry 40*, 7180−7191.
(34) Zhang, X., Lee, I., and Berdis, A. J. (2005) The use of nonnatural nucleotides to probe the contributions of shape complementarity and π-electron surface area during DNA polymerization. *Biochemistry 44*, 13101−13110.
(35) Zhang, X., Lee, I., Zhou, X., and Berdis, A. J. (2006) Hydrophobicity, shape, and π-electron contributions during translesion DNA synthesis. *J. Am. Chem. Soc. 128*, 143−149.
(36) Wang, M., Xia, S., Blaha, G., Steitz, T. A., Konigsberg, W. H., and Wang, J. (2011) Insights into base selectivity from the 1.8 Å resolution structure of an RB69 DNA polymerase ternary complex. *Biochemistry 50*, 581−590.
(37) Berman, A. J., Kamtekar, S., Goodman, J. L., Lazaro, J. M., de Vega, M., Blanco, L., Salas, M., and Steitz, T. A. (2007) Structures of phi29 DNA polymerase complexed with substrate: The mechanism of translocation in B-family polymerases. *EMBO J. 26*, 3494−3505.
(38) Xia, S., Eom, S. H., Konigsberg, W. H., and Wang, J. (2012) Structural Basis for Differential Insertion Kinetics of dNMPs Opposite a Difluorotoluene Nucleotide Residue. *Biochemistry 51*, 1476−1485.
(39) McCoy, A. J., Grosse-Kunstleve, R. W., Adams, P. D., Winn, M. D., Storoni, L. C., and Read, R. J. (2007) Phaser crystallographic software. *J. Appl. Crystallogr. 40*, 658−674.
(40) Murshudov, G. N., Vagin, A. A., and Dodson, E. J. (1997) Refinement of macromolecular structures by the maximum-likelihood method. *Acta Crystallogr. D53*, 240−255.
(41) Emsley, P., and Cowtan, K. (2004) Coot: Model-building tools for molecular graphics. *Acta Crystallogr. D60*, 2126−2132.
(42) *The PyMOL Molecular Graphics System*, version 1.2r3pre (2010) Schrodinger, LLC, New York.
(43) Xia, S., Konigsberg, W. H., and Wang, J. (2011) Hydrogen-bonding capability of a templating difluorotoluene nucleotide residue in an RB69 DNA polymerase ternary complex. *J. Am. Chem. Soc. 133*, 10003−10005.
(44) Wang, M., Xia, S., Blaha, G., Steitz, T. A., Konigsberg, W. H., and Wang, J. (2011) Insight into base selectivity from the 1.8Å resolution structure of an RB69 DNA polymerase ternary complex. *Biochemistry 50*, 581−590.
(45) Nair, D. T., Johnson, R. E., Prakash, L., Prakash, S., and Aggarwal, A. K. (2009) DNA synthesis across an abasic lesion by human DNA polymerase ι. *Structure 17*, 530−537.
(46) Wang, F., and Yang, W. (2009) Structural insight into translesion synthesis by DNA Pol II. *Cell 139*, 1279−1289.
(47) Ling, H., Boudsocq, F., Woodgate, R., and Yang, W. (2004) Snapshots of replication through an abasic lesion; structural basis for base substitutions and frameshifts. *Mol. Cell 13*, 751−762.